Inverse method for the determination of a mathematical expression for the anisotropy of the solid-liquid interfacial energy in Al-Zn-Si alloys

C. Niederberger,[1,2,*] J. Michler,[2,†] and A. Jacot[1,‡]

[1]*Computational Materials Laboratory, Institute of Materials, Ecole Polytechnique Fédérale de Lausanne, Station 12, CH-1015 Lausanne, Switzerland*

[2]*Swiss Federal Laboratories for Materials Testing and Research (EMPA), Feuerwerkerstrasse 39, CH-3602 Thun, Switzerland*

(Received 10 April 2006; published 23 August 2006; publisher error corrected 29 August 2006)

An expression for the anisotropy of the solid-liquid interfacial energy has been determined experimentally by an inverse method for the Al-43.4 wt %Zn-1.6 wt %Si system. Assuming that dendrite growth directions correspond to the minima of the surface stiffness, the anisotropy of the solid-liquid interfacial energy could be described by minimizing the errors between the calculated minima of a parametric interface stiffness function and experimentally measured growth directions of dendrites in thin coatings. In order to adequately describe the interfacial energy, it is found that a cubic harmonic expansion up to the third order is necessary to obtain the minima of interface stiffness along directions that depart from ⟨100⟩ or ⟨110⟩. Best agreement with observed growth directions is obtained for first, second, and third harmonic coefficients (ε_1, ε_2, and ε_3, respectively) satisfying the following relationships: $\varepsilon_2/\varepsilon_1=-0.188$; $\varepsilon_3/\varepsilon_1=-0.00776$. The corresponding interface stiffness function shows 24 minima lying along directions between ⟨100⟩ and ⟨110⟩. The minima are located at 28.5° from ⟨100⟩ and only 5.1° from ⟨320⟩, which was the growth direction suggested by Sémoroz *et al.* for this alloy [A. Sémoroz, Y. Durandet, and M. Rappaz, Acta Mater. **49**, 529 (2001).]. It was also found that the strength of the effective in-plane anisotropy is directly reflected by the morphology of the dendritic microstructure.

DOI: 10.1103/PhysRevE.74.021604 PACS number(s): 68.70.+w, 81.30.Fb, 47.20.Dr

I. INTRODUCTION

Pattern formation during solidification is a topic of considerable interest from both scientific and technological points of view, and has been the subject of intensive research over the past decades [1,2]. A key quantity in the selection of the solidification morphology is the solid-liquid interfacial energy and its anisotropy, i.e., its dependence on the local crystallographic orientation of the solid-liquid interface. The anisotropy of the interfacial energy, even in nonfaceted metallic systems where it is as small as 1% typically, plays an important role in pattern formation. It is first responsible for the fact that dendrites grow in a structured way and generally exhibit well-defined angles—most often 90° in cubic systems—between the primary and secondary arms. It was shown both experimentally and theoretically that a decrease in the magnitude of the anisotropy of the interfacial energy leads to a transition from stable dendritic structures growing along preferred crystallographic directions to unstructured seaweed patterns [3,4]. Moreover, it is now well established that the operating state of a dendrite tip is significantly affected by the anisotropy of the solid-liquid interfacial energy as predicted by microscopic solvability theory [5,6] and confirmed recently by numerical simulations [7].

With the emergence of quantitative numerical methods for the simulation of solidification microstructures—namely the phase-field method [8,9]—needs have become more acute to collect data of the solid-liquid interfacial energy and to formulate mathematical expressions describing its anisotropy. In recent years, significant progress has been made in that sense through molecular dynamics simulations [10–14] and experimental techniques [15–17]. Among the simulation techniques recently reviewed by Hoyt *et al.* [10], two methods have been applied with success. The first calculates the work required to create a solid-liquid interface [13,14] and the second evaluates the fluctuations of the level of the crystal-melt interface which are directly related to the surface stiffness [10,11]. Experimental measurements of the anisotropy of the solid-liquid interfacial energy have been done through the determination of the equilibrium shape of a solid crystal in a melt in the case of transparent organic alloys [18,19] and more recently through serial sectioning of quenched liquid droplets in metallic systems [15–17]. Herefore, the equilibrium shape is related to the solid-liquid interfacial energy through the so-called Wulff construction. Such experiments require extreme caution as the anisotropy of the interfacial energy is small and the equilibrium shapes are nearly spherical. Nevertheless, reliable measurements have been reported in the (001) crystallographic plane for Al-Cu [15] and Al-Si [15,16] and in three dimensions for the Al-Sn system [17].

In metals of cubic crystal structure, dendrite tips grow in most cases along the ⟨100⟩ orientations. Formulating a mathematical expression for the dependence of the surface energy upon interface orientation is relatively straightforward in that case and is naturally obtained with spherical harmonics satisfying the cubic symmetry. This mathematical form has been implemented in phase-field simulations [8] and was used also by Napolitano and Liu [17] to characterize their experimental data. It has been reported that dendrites of the fcc structure can grow along directions that differ from

*Email address: christoph.niederberger@epfl.ch
†Email address: johann.michler@empa.ch
‡Email address: alain.jacot@epfl.ch

⟨100⟩. Dendritic growth along ⟨110⟩ directions was observed by Henry in Al-Mg-Mn [20,21] and by Napolitano in Al-Si-Sr [16], while Sémoroz *et al.* observed growth along orientations close to ⟨320⟩ in Al-Zn-Si alloys [22]. Very recently, Gonzales *et al.* reported the continuous transition from ⟨100⟩ to ⟨110⟩ growth with increasing Zn content in the binary Al-Zn system [23].Even though the possible influence of anisotropic attachment kinetics cannot be totally excluded, as the dendrites grow at finite speed, the reported results indicate that the interfacial energy is a complex function of crystal orientation and composition, which remains to be established.

The objective of the present work is to propose an inverse method for the determination of a mathematical function describing the anisotropy of the solid-liquid interfacial energy, based on the observation of dendritic patterns in thin coatings. The method is applied to the Al-43.4 wt %Zn-1.6 wt %Si system for which evidences of dendritic growth along directions close to ⟨320⟩ have been reported [22]. It is also used to determine more accurately the preferred crystallographic growth direction in this alloy.

II. BACKGROUND

The influence of the interfacial energy on the equilibrium and dynamics of a solid-liquid interface in an alloy can be quantified with the generalized Gibbs-Thomson relation:

$$T = T_{liq}(c_{liq}) - \Delta T_r - \Delta T_k \tag{1}$$

which expresses the interface temperature T as a function of the local liquid concentration c_{liq}, curvature undercooling ΔT_r, and kinetic undercooling ΔT_k. In Eq. (1), $T_{liq}(c_{liq})$ expresses the liquidus temperature as a function of the concentration. For isotropic interfaces, the curvature undercooling can be expressed as

$$\Delta T_r = \frac{\gamma_{sl}}{\Delta S_f}\kappa = \Gamma\kappa, \tag{2}$$

where κ is the local interface curvature, γ_{sl} is the solid-liquid interfacial energy, ΔS_f is the entropy of melting, and Γ is the Gibbs-Thomson coefficient. The kinetic undercooling, ΔT_k, is given by:

$$\Delta T_k = \frac{\nu}{\mu}, \tag{3}$$

where ν is the interface velocity and μ is the mobility coefficient.

The undercooling terms ΔT_r and ΔT_k are related to intrinsic interfacial properties, the Gibbs-Thomson and mobility coefficients, which are anisotropic in nature, i.e., they depend on the local crystallographic orientation of the solid-liquid interface. If the anisotropy of the interfacial energy can be expressed as a function of the normal vector to the interface, **n**, the curvature undercooling can be written as [24]

$$\Delta T_r(\mathbf{n}) = \frac{1}{\Delta S_f}\left[\kappa_1\left(\gamma_{sl}(\mathbf{n}) + \frac{\partial^2\gamma_{sl}(\mathbf{n})}{\partial\vartheta_1^2}\right) + \kappa_2\left(\gamma_{sl}(\mathbf{n}) + \frac{\partial^2\gamma_{sl}(\mathbf{n})}{\partial\vartheta_2^2}\right)\right], \tag{4}$$

where κ_1 and κ_2 are the principal curvatures of the solid-liquid interface. The terms in the parentheses are the two principal interface stiffness components. They involve the second partial derivatives of $\gamma_{sl}(\mathbf{n})$ in the planes associated with the corresponding principal curvatures by which they are multiplied.

Under the assumption of a locally spherical interface, i.e. $\kappa_1 = \kappa_2 = \kappa/2$, Eq. (4) becomes [17]

$$\Delta T_r(\mathbf{n}) = \kappa\Gamma^0\Phi_r(\mathbf{n}),$$

$$\Phi_r(\mathbf{n}) = \frac{1}{\gamma_{sl}^0}\left[\gamma_{sl}(\mathbf{n}) + \frac{1}{2}\left(\frac{\partial^2\gamma_{sl}(\mathbf{n})}{\partial\vartheta_1^2} + \frac{\partial^2\gamma_{sl}(\mathbf{n})}{\partial\vartheta_2^2}\right)\right], \tag{5}$$

where $\Gamma^0 = \gamma_{sl}^0/\Delta S_f$ is a mean Gibbs-Thomson coefficient and $\Phi_r(\mathbf{n})$ is the normalized generalized interface stiffness as defined in Ref. [17], which is a scalar function of the local interface orientation and can readily be calculated if $\gamma_{sl}(\mathbf{n})$ is known.

In general, the interface stiffness is more anisotropic than the interfacial energy. This statement is easily verified by considering the mathematical form commonly used to describe the weak anisotropy of cubic crystals in the {100} planes as a function of the angle θ between **n** and the [100] direction:

$$\gamma_{sl}(\theta) = \gamma_0(1 + \varepsilon\cos 4\theta) \tag{6}$$

from which one deduces immediately that the anisotropy of the interface stiffness, $\gamma_{sl} + \mathrm{d}^2\gamma_{sl}/\mathrm{d}\theta^2$ is 15 times larger than that of γ_{sl}.

The interface stiffness derived from Eq. (6) exhibits minima along ⟨100⟩ directions which correspond exactly to the maxima of γ_{sl}. For more complex anisotropy functions however, this property is not necessarily verified [25].

Assuming that equiaxed dendritic solidification starts from a spherical nucleus, the curvature undercooling is not constant on the solid-liquid interface since it varies as described by Eq. (5). Neglecting the kinetic undercooling, which is usually very small in metallic systems under normal solidification conditions, the driving force for solidification will be highest where the curvature undercooling is lowest, i.e., at the minima of the interface stiffness if spherical interfaces are assumed. As a consequence, the solid-liquid interface will form protrusions which will develop naturally into dendrite tips as soon as the conditions for interface destabilization are met. One can, therefore, assume that the dendrite arms grow along the orientations where the generalized interfacial stiffness, $\Phi_r(\mathbf{n})$, exhibits minima. It could be argued that dendrite growth directions are rather determined by the most prominent protrusions of the equilibrium shape of the crystal, which is defined as the shape that exhibits equal curvature undercooling for all points on the solid-liquid interface. As the equilibrium shape is not a sphere for aniso-

tropic interfaces, the simplified form of Eq. (4) can, in principle, not be used to calculate it. However, the most prominent protrusions of the equilibrium shape probably have, locally, similar main radii of curvature, κ_1 and κ_2, which can justify the simplification made in Eq. (5). Moreover, due to the dynamics of the process, it is quite likely that the equilibrium shape is never fully established. For simplicity, the assumption that dendrites grow along the directions that correspond to the minimum, the generalized interface stiffness, $\Phi_r(\mathbf{n})$, will subsequently be used throughout the present paper.

The orientation dependence of $\gamma_{sl}(\mathbf{n})$ in three dimensions is described as an expansion of cubic harmonics, which are a basis set of linear combinations of spherical harmonics that respect the cubic symmetry of the crystal lattice [26]. The anisotropic character of the solid-liquid interfacial energy can be expressed as

$$\gamma_{sl}(\mathbf{n}) = \gamma_{sl}^0 \left[\begin{array}{l} 1 + \varepsilon_1 \left(Q - \frac{3}{5} \right) + \varepsilon_2 \left(3Q + 66S - \frac{17}{7} \right) \\ + \varepsilon_3 (65Q^2 - 94Q - 208S + 33) + \cdots \end{array} \right], \quad (7)$$

where

$$Q = n_x^4 + n_y^4 + n_z^4, \quad (8)$$

$$S = n_x^2 n_y^2 n_z^2, \quad (9)$$

n_x, n_y, and n_z are the Cartesian components of the unit normal vector to the solid-liquid interface expressed in the crystallographic coordinate system. In most studies, the interfacial anisotropy has been described by expansions up to the second order, i.e., the coefficients ε_3 and higher have been neglected. This allowed us to describe accurately the solid-liquid interfacial energy in systems such as Al-Cu [27] by numerical simulation or in Al-Sn [17] by experimental determination of the equilibrium shape. In both cases positive values have been determined for ε_1 and negative values for ε_2. If the interface stiffness $\Phi_r(\mathbf{n})$ is expressed by the first two cubic harmonics, it exhibits either minima along the $\langle 100 \rangle$ orientations if $\varepsilon_2 > -0.15\varepsilon_1$ or along $\langle 110 \rangle$ if $\varepsilon_2 < -0.15\varepsilon_1$. In order to describe interfacial energies leading to minima of the stiffness along directions within $\{100\}$ planes but other than $\langle 100 \rangle$ and $\langle 110 \rangle$, we propose to include the ε_3 term in the cubic harmonics expansion of the interfacial energy, Eq. (7).

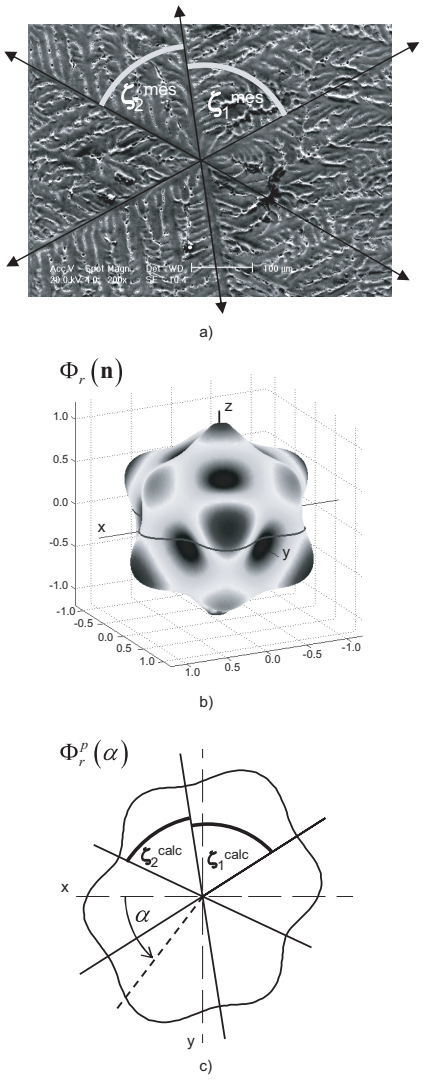

FIG. 1. (a) Typical microstructure obtained a few microns underneath the surface of an Al-Zn-Si coating and used for the determination of the ζ^{mes} angles. (b) Computed stiffness plot for the crystallographic orientations of the grain shown in (a). The coordinate axes correspond to the coordinate system of the sample where z is normal to the coating plane. The circumferential line in the (x,y) plane corresponds to the intersection of the stiffness plot with the coating plane. (c) The local minima of the in-plane stiffness plot allow determining of the ζ^{calc} angles. The anisotropy parameters have been arbitrarily selected ($\varepsilon_1=0$, $\varepsilon_2=0.01$, $\varepsilon_3=0$) for this figure.

III. DESCRIPTION OF THE METHOD

The method used to characterize the anisotropy of the interfacial energy is based on the observation of dendrite growth directions in thin coatings. The selected system consists of Al-43.4 wt %Zn-1.6 wt %Si coatings deposited on a steel substrate by the hot dipping process, which exhibit a thickness between 20 and 30 μm. The microstructure of such coatings is composed of Al-rich dendrites of the fcc crystal structure, Fig. 1(a). The primary phase is believed to nucleate on the interface between the substrate and the coating, before developing dendrite arms which detach from the coating-substrate interface and propagate within the liquid film [28]. As the preferred crystallographic dendrite growth directions are, in general, not aligned with the plane of the coating and as the coating is thin, the dendrite tips are forced to grow along the two boundaries confining the melt. The growth directions of the dendrites that are visible at the free surface (or in a parallel section a few microns underneath) do not necessarily correspond to the crystallographic growth directions of a dendrite growing in the bulk, i.e., the global minima of the interface stiffness. In fact, it is much more plausible that the dendrite tips grow along the directions that correspond to local minima of the surface stiffness within the

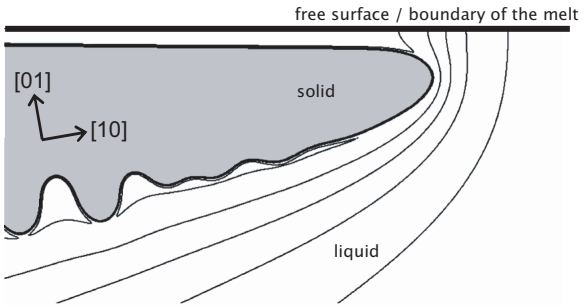

FIG. 2. 2D Phase field simulation of a dendrite tip growing along a boundary confining the melt. A solute-rich liquid layer remains between the dendrite tip and the boundary even though the crystallographic growth direction [10] is pointing towards the boundary.

coating plane. This concept is illustrated in Fig. 1(b) which displays a typical three-dimensional interface stiffness plot having the same orientation with respect to the coating plane as the grain of Fig. 1(a). The local minima within the plane of the coating, which are determined from the trace of the stiffness plot in this plane, [see Fig. 1(c)], correspond well to the growth directions observed in Fig. 1(a).

The assumption that the dendrite tips grow along the in-plane minima of the interface stiffness relies also on recent experimental observations and phase-field simulations which gave evidences that the dendrite tips remain separated from the confining boundaries by a thin layer of solute enriched liquid (see Fig. 2) [28]. Since the dendrite tips are separated from the boundaries confining the coating, the interfacial energies between the solid and the substrate or between the solid and the free surface should not influence the dendrite tip kinetics.

Experimental observations have shown that either six or eight primary dendrite branches are present in the plane of the coating [22]. The number of growth directions and the angles between them, $\{\zeta^{mes}\}$, depend of the crystallographic orientation of the growing grain with respect to the coating plane. In the case of six growth directions, two angles, ζ_1^{mes} and ζ_2^{mes}, completely describe the orientation of the growth directions with respect to each other [see Fig. 1(a)]. In the case of eight growth directions, three angles are required.

For a given grain orientation and a given set of coefficients of the cubic harmonic expansion, $\boldsymbol{\varepsilon}=(\varepsilon_1,\varepsilon_2,\varepsilon_3)$, the angles between the expected growth directions in the coating plane, $\{\zeta^{calc}(\boldsymbol{\varepsilon})\}$, can be obtained by determining the local minima in the corresponding plane of the stiffness plot (see Fig. 1).

More precisely, the growth directions in the coating plane are obtained by solving the following equation:

$$\frac{d\Phi_r^p(\alpha)}{d\alpha}=0 \quad \text{with} \quad \frac{d^2\Phi_r^p(\alpha)}{d\alpha^2}>0, \tag{10}$$

where $\Phi_r^p(\alpha)$ expresses the trace of the interface stiffness in the coating plane as a function of the in-plane polar angle α [see Fig. 1(c)].

This function is obtained by operating the following coordinate change:

$$\Phi_r^p(\alpha)=\Phi_r[\mathbf{n}(\alpha)]=\Phi_r\left[[\mathbf{M}]\cdot\begin{pmatrix}\cos\alpha\\ \sin\alpha\\ 0\end{pmatrix}\right], \tag{11}$$

where $\Phi_r(\mathbf{n})$ is the normalized generalized interface stiffness expressed in the crystallographic coordinate system and defined by Eqs. (5) and (7)–(9). The matrix $[\mathbf{M}]$ is a transformation matrix describing the transition from the sample coordinate system to the crystallographic coordinate system. It is given by:

$$[\mathbf{M}]=\begin{pmatrix}\cos\varphi_2 & \sin\varphi_2 & 0\\ -\sin\varphi_2 & \cos\varphi_2 & 0\\ 0 & 0 & 1\end{pmatrix}\cdot\begin{pmatrix}1 & 0 & 0\\ 0 & \cos\phi & \sin\phi\\ 0 & -\sin\phi & \cos\phi\end{pmatrix}\cdot\begin{pmatrix}\cos\varphi_1 & \sin\varphi_1 & 0\\ -\sin\varphi_1 & \cos\varphi_1 & 0\\ 0 & 0 & 1\end{pmatrix}, \tag{12}$$

where φ_1, ϕ, φ_2 are the three Euler angles of the grain which are generally used to describe the crystallographic orientation of a grain with respect to the sample coordinate system. In our case, the z axis of the sample coordinate system is normal to the plane of the coating. The three Euler angles can be obtained from electron backscattering diffraction (EBSD) measurements. The solution of Eq. (10) is obtained numerically using a very fine mapping of $\Phi_r^p(\alpha)$.

By applying the procedure described above for a series of grains, an inverse method can be formulated in order to determine the most relevant set of anisotropy coefficients. Following the inverse method described in [29] for another optimization problem, the procedure consists of looking for the anisotropy coefficients, $\boldsymbol{\varepsilon}=(\varepsilon_1,\varepsilon_2,\varepsilon_3)$, which minimize the mean square deviation $S(\boldsymbol{\varepsilon})$ between measured angles $\{\zeta^{mes}\}$ and calculated angles $\{\zeta^{calc}\}$:

$$S(\boldsymbol{\varepsilon})=\sum_{i=1}^{N}[\zeta_i^{mes}-\zeta_i^{calc}(\boldsymbol{\varepsilon})]^2, \tag{13}$$

where N is the number of angles that have been determined experimentally.

As the locations of the minima of the stiffness plot only depend on the relative magnitude of the anisotropy coefficients and not on their absolute values, the condition for a

TABLE I. Euler angles as well as measured and calculated ζ angles for the individual grains used in the inverse method analysis.

	φ_1	ϕ	φ_2	ζ^{mes}	ζ^{calc}
Grain 1	118.1	52.0	39.9	67.5	71.75
				47.5	44.00
Grain 2	230.6	31.1	55.7	41.4	37.50
				65.0	66.75
Grain 3	38.4	9.8	45.4	25.0	31.25
				54.5	56.75
				46.5	35.25
Grain 4	83.7	13.5	40.8	30.0	33.50
				39.5	45.00
				50.5	50.00
Grain 5	142.1	32.0	85.2	74.0	74.25
				41.0	36.25

local minimum can be expressed as a function of only two anisotropy parameters:

$$\frac{\partial S}{\partial \varepsilon_2} = 0,$$

$$\frac{\partial S}{\partial \varepsilon_3} = 0. \tag{14}$$

The minimum of S is obtained by an iterative descent algorithm [29], which consists of linearizing $\zeta_i^{calc}(\boldsymbol{\varepsilon})$ and using numerical estimations of the sensitivity coefficients, $\partial\zeta_i^{calc}/\partial\varepsilon_2$ and $\partial\zeta_i^{calc}/\partial\varepsilon_3$ to calculate the increments of ε_2 and ε_3 between two successive iterations. As the method involves only two out of the three anisotropy coefficients, it does not allow for the determination of the absolute magnitude of the anisotropy. The objective is, therefore, restricted to the determination of the shape of the interface stiffness and interfacial energy functions.

IV. RESULTS

In the present work, a set of five randomly selected grains has been investigated. The crystallographic orientations of the grains were determined by EBSD. The Euler angles have been reported in Table I, and the inverse pole figure of Fig. 3 shows the orientation of the normal to the coating plane in the crystallographic reference frames of the five grains. Three grains exhibit six primary growth directions while the two others show eight primary arms, which leads thereby to a total number of $N=12$ measured angles, ζ^{mes}.

The inverse method was applied to this set of data, starting with the following initial guess for the anisotropy parameters: $\varepsilon_1=0.025$, $\varepsilon_2=-0.007$, and $\varepsilon_3=-0.0005$. Keeping ε_1 constant, the iterative procedure converged towards $\varepsilon_2=-0.00469$ and $\varepsilon_3=-0.000194$, which corresponds to the following ratios: $\varepsilon_2/\varepsilon_1=-0.188$ and $\varepsilon_3/\varepsilon_1=-0.00776$. Tests have shown that the initial choice for $\boldsymbol{\varepsilon}$ has no influence on the solution as long as it is chosen within reasonable limits,

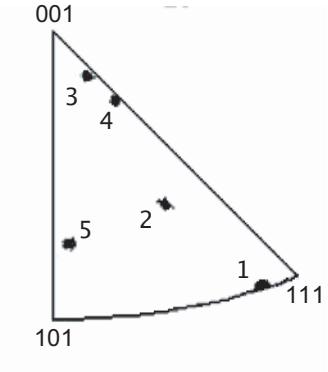

FIG. 3. Inverse pole figure giving the orientation of the normal to the coating plane in the crystallographic reference frame of the five grains used for the inverse method analysis.

e.g., $\Phi_r(\mathbf{n})>0\ \forall\mathbf{n}$, which is the condition for nonfacetted crystal growth. The interfacial energy $\gamma_{sl}(\mathbf{n})/\gamma_{sl}^0$ and the normalized general stiffness $\Phi_r(\mathbf{n})$ corresponding to the optimized anisotropy parameters are shown in Fig. 4. The calculated growth direction angles ζ^{calc} corresponding to this anisotropy function are given in Table I, where they can be compared to the corresponding measured angles ζ^{mes}.

V. DISCUSSION

The interfacial energy shown in Fig. 4(a) as a function of the interface orientation exhibits its lowest value for interfaces having their normal corresponding approximately to the $\langle 111\rangle$ directions, i.e., for interfaces that are parallel to the dense packed planes of the fcc structure. The maximum of interfacial energy is observed for $\{100\}$ interfaces, whereas saddle points are found for $\{110\}$. The sections through the $\gamma_{sl}(\mathbf{n})$ plots shown in Fig. 4(b)–4(d) indicate that the amplitude of the anisotropy in a given plane strongly depends on its orientation. The interfacial energy within the $(\bar{1}10)$ plane [Fig. 4(c)] exhibits two global maxima of the [001] family and four global minima of the [111] family. For sections that are parallel to the (001) plane [Fig. 4(b)], however, the in-plane anisotropy is substantially weaker as the difference of interfacial energy between [100] and [110] is considerably smaller than between [001] and [111]. The in-plane anisotropy of $\gamma_{sl}(\mathbf{n})$ is even weaker within the (111) section [Fig. 4(d)].

The present case is an example of an interfacial energy function whose maxima do not correspond to the minima of the surface stiffness. The stiffness plot exhibits global maxima along $\langle 111\rangle$ and local maxima along $\langle 100\rangle$ [Fig. 4(e)]. Again, saddle points can be found for the $\langle 110\rangle$ orientations. The global minima of the stiffness are, however, located between the $\langle 100\rangle$ and $\langle 110\rangle$ directions, forming a 28.5° angle with the $\langle 100\rangle$ orientations. This result is in agreement with the recent observations of Gonzales *et al.* [17] who showed that the preferential dendritic growth direction gradually changes form $\langle 100\rangle$ to $\langle 110\rangle$ as the Zn concentration is increased in a binary Al-Zn alloy. For an Al-50 wt %Zn, they reported growth directions 32.7° off the

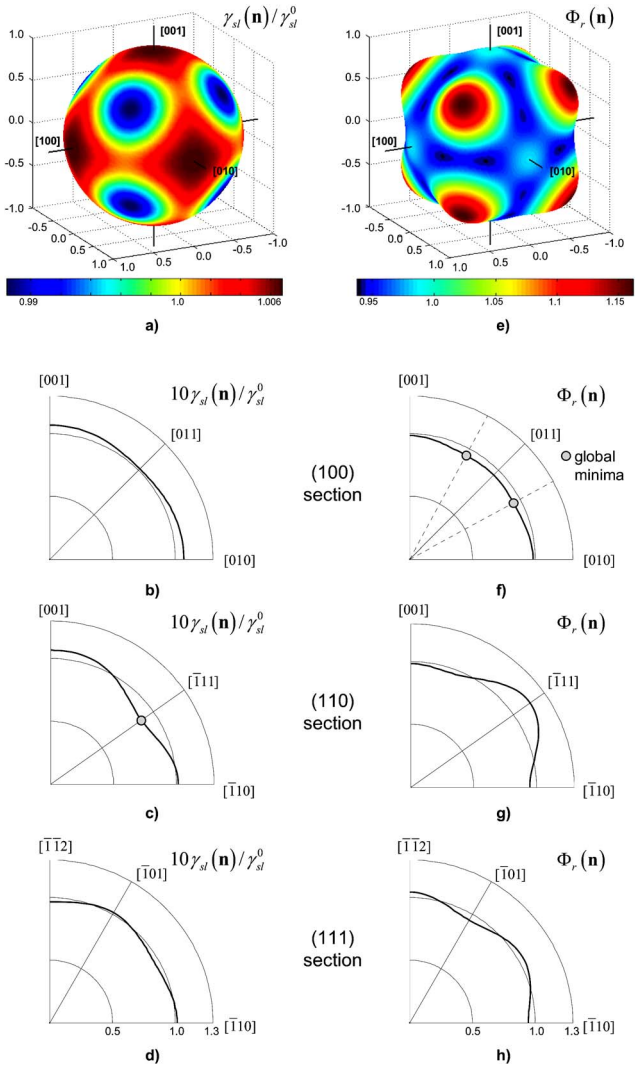

FIG. 4. (Color online) Plots of $\gamma_{sl}(\mathbf{n})/\gamma_{sl}^0$ (a) and $\Phi_r(\mathbf{n})$ (e) vs crystallographic orientation for the optimized values of anisotropy $\varepsilon_2=-0.188\,\varepsilon_1$ and $\varepsilon_3=-0.00776\,\varepsilon_1$ with $\varepsilon_1=0.025$. The maxima of the interfacial energy are reached for the ⟨100⟩ directions whereas the minima of the stiffness are located in between ⟨100⟩ and ⟨110⟩. The coordinate axes correspond to the crystallographic ⟨100⟩ directions. 2D sections of interfacial energy and stiffness are given in (b) and (f), respectively, for the (001) plane, in (c) and (g) for the (110) plane, and in (d) and (h) for the (111) plane. For the 2D plots of the interfacial energy (b)–(d), the magnitude of the anisotropy was increased by a factor of 10 as no minima and maxima are discernable otherwise. The 2D plots of the interface stiffness (e)–(g) were not amplified.

⟨100⟩ orientations. In consequence, there are in total 24 minima of the stiffness and hence also 24 possible dendritic growth directions. The 2D section through the stiffness plot shown in Fig. 4(f) clearly reveals that the in-plane anisotropy is very weak for {001} sections.

Since the dendrites are confined to grow in the thin coating layer, the selected growth pattern does not only depend on ε_1, ε_2, and ε_3 but also on the orientation of the crystal with respect to the coating plane. As mentioned above, the dendrites in the coating layer are assumed to grow along the

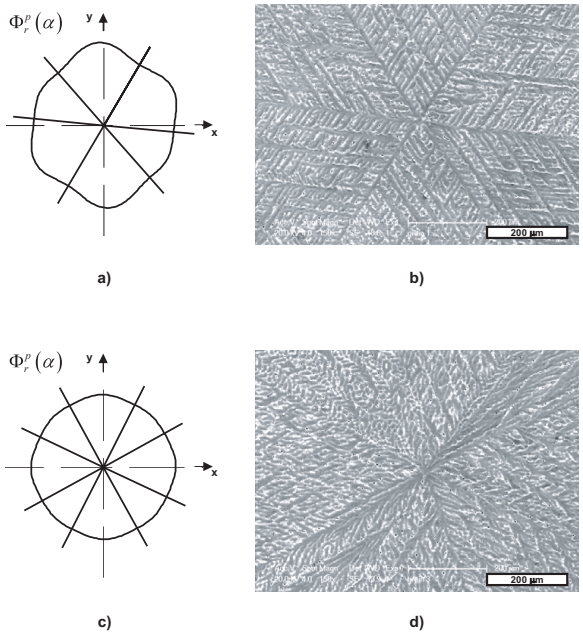

FIG. 5. (a) In-plane stiffness plot for a grain having a {111} crystallographic plane close to the coating plane. The minima of the stiffness are highlighted by the radial lines. (b) The micrograph of the corresponding grain shows a well-defined dendrite structure. (c) In-plane stiffness plot for a grain having a {100} crystallographic plane close to the coating plane. The anisotropy is weaker than in (a) and leads to a dendrite pattern with poorly defined growth directions (d).

directions for which the intersection of the stiffness plot and the plane of the coating exhibits local minima. Depending on the crystallographic orientation with respect to the coating, the magnitude of this in-plane anisotropy may be very variable. Strong in-plane anisotropy is observed for crystals having a {110} [Fig. 4(g)] or {111} [(Fig. 4(h)] crystallographic plane nearly parallel to the coating plane. In this case, the microstructure shows a very well-defined dendritic pattern with six dendrite growth directions that can be distinctly identified. An example of a grain having the (111) plane almost aligned with the coating plane is given in Figs. 5(a) and 5(b) (the exact orientation of this grain can be seen in Fig. 3 where it is labeled "1"). If, however, a {100} plane is approximately parallel to the coating plane (grain 3 on Fig. 3), the effective in-plane anisotropy is much weaker and eight minima of the stiffness are present [see Fig. 5(c)]. On the corresponding micrograph [Fig. 5(d)], eight dendrite growth directions can be identified, but the dendrite growth directions are sometimes blurred and smooth transitions form one growth direction to another seem to be possible. This corresponds well to the weak effective in-plane anisotropy observed for surface stiffness in the (100) plane [Fig. 4(f)]. Similarly, planes of strong and weak effective in-plane anisotropy have been reported in the literature for transparent organic alloys of cubic crystal structure [3,4] by *in situ* observation of solidification in thin layers. The planes of strong and weak effective anisotropy are however, different, in the reported organic systems as compared to the Al-Zn-Si alloy considered here. In CBr_4-C_2Cl_6 [3] and succinonitrile [4]

thin samples, dendritic growth with distinctly pronounced arm directions is found if the sample plane is aligned with a {100} crystallographic plane. If, however, the sample is aligned with a {111} plane, unsteady seaweed growth is observed as the anisotropy of the stiffness vanishes for this orientation. A cubic harmonics expansion considering only ε_1 and neglecting higher order terms describes, therefore, well the anisotropy of the interfacial energy in the mentioned organic alloys, as a first order expansion leads to pronounced anisotropy in the {100} planes but to no anisotropy in the {111} planes [4]. The behavior of the Al-Zn-Si alloy is considerably different as this system shows well-defined dendrite pattern in {111} and {110} sections and more blurred dendrites in {100} sections. This confirms the necessity to consider the additional ε_2 and ε_3 contributions in this system.

The calculated and measured growth directions reported in Table I show good agreement, if one considers the errors associated with the measurements (estimated at a few degrees). The fact that the dendritic morphologies observed in the coating plane [Figs. 5(b) and 5(d)] are in accordance with the in-plane anisotropy of the interface stiffness further validate the results. However, one should bear in mind that the assumption of dendritic growth along directions corresponding to minima of the generalized interface stiffness, $\Phi_r(\mathbf{n})$, is not universally valid as it is based on the assumption of equal main radii of interface curvature at the dendrite tip. Moreover, the shape and hence the growth direction of a dendrite tip are determined by an interplay of the capillary and diffusional aspects. Therefore, to better establish the relationship between interfacial energy and/or surface stiffness and the observed growth directions quantitative 3D phase-field simulations would be required.

VI. CONCLUSION

An inverse method for the determination of a mathematical expression for the anisotropy of the solid-liquid interfacial energy has been developed. The method is based on the observation of dendritic microstructures in thin coatings. Assuming that dendrites grow along crystallographic directions corresponding to minima of the generalized interface stiffness, a function describing the anisotropy of the solid-liquid interfacial energy could be determined. In order to describe the anisotropy in Al-43.4 wt %Zn-1.6% Si alloy, the interfacial energy was expanded in terms of a cubic harmonics series. The second order expansion previously reported for other alloy systems does not provide a correct description of the anisotropy in Al-Zn-Si systems. Therefore an expansion to the third order was introduced. Best agreement with observed growth directions was obtained for first, ε_1, second, ε_2, and third, ε_3, harmonic coefficients satisfying the following relationships: $\varepsilon_2/\varepsilon_1=-0.188$; $\varepsilon_3/\varepsilon_1=-0.00776$. The interfacial energy reaches its maximum for solid-liquid interfaces having their normal aligned with the $\langle 100\rangle$ direction. The surface stiffness shows minima lying between the $\langle 100\rangle$ and $\langle 110\rangle$ directions, and 28.5° away form the $\langle 100\rangle$ orientations. The present function illustrates, therefore, well that the maxima of the interfacial energy do not necessarily correspond to the minima of the interface stiffness in nonfaceted alloys. The morphology of dendrites constrained to grow in a coating plane is related to the magnitude of the effective in-plane anisotropy, which depends on the relative orientation of the crystal with respect to the coating plane. For Al-43.4 wt %Zn-1.6 %Si, if the coating plane is aligned with the {110} or {111} crystallographic planes, the in-plane anisotropy is pronounced, and a well-defined dendritic pattern is adopted. If a {100} plane is aligned with the coating, the in-plane anisotropy is considerably weaker and dendrite growth directions become blurred which is in good accordance with the expression determined for the solid-liquid interfacial energy.

Although the absolute magnitude of the anisotropy cannot be determined by the present method, a mathematical function for the surface energy is of avail for numerical simulation of the Al-43.4 %Zn-1.6 wt %Si solidification microstructures by phase-field or alternate methods.

ACKNOWLEDGMENTS

The authors would like to thank Professor M. Rappaz for reading the manuscript and the valuable comments. Financial support from the research commissions of the Ecole Polytechnique Fédérale de Lausanne (EPFL), Switzerland, and of the Swiss Federal Institute for Materials Testing (EMPA), Switzerland, is greatly acknowledged.

[1] W. J. Boettinger, S. R. Coriell, A. L. Greer, A. Karma, W. Kurz, M. Rappaz, and R. Trivedi, Acta Mater. **48**, 43 (2000).
[2] *Solidification processes and microstructures: A Symposium in Honor of Wilfried Kurz*, edited by M. Rappaz, C. Beckermann, and R. Trivedi (TMS, Warrendale, 2004).
[3] S. Akamatsu, G. Faivre, and T. Ihle, Phys. Rev. E **51**, 4751 (1995).
[4] B. Utter and E. Bodenschatz, Phys. Rev. E **66**, 051604 (2002).
[5] H. Müller-Krumbhaar and W. Kurz, in *Phase Transformations in Materials*, edited by P. Haasen (VCH, Weinheim, 1991), p. 553.
[6] D. A. Kessler, J. Koplik, and H. Levine, Adv. Phys. **37**, 255 (1988).
[7] A. Karma and W.-J. Rappel, J. Cryst. Growth **174**, 54 (1997).
[8] A. Karma and W.-J. Rappel, Phys. Rev. E **57**, 4323 (1998).
[9] W. J. Boettinger, J. A. Warren, C. Beckermann, and A. Karma, Annu. Rev. Mater. Res. **32**, 163 (2002).
[10] J. J. Hoyt, M. Asta, and A. Karma, Mater. Sci. Eng., R. **41**, 121 (2003).
[11] J. J. Hoyt, M. Asta, and A. Karma, Phys. Rev. Lett. **86**, 5530 (2001).
[12] J. R. Morris and R. E. Napolitano, JOM **56**, 40 (2004).

[13] R. L. Davidchack and B. B. Laird, Phys. Rev. Lett. **85**, 4751 (2000).
[14] B. B. Laird and R. L. Davidchack, J. Phys. Chem. B **109**, 17802 (2005).
[15] S. Liu, R. E. Napolitano, and R. Trivedi, Acta Mater. **49**, 4271 (2001).
[16] R. E. Napolitano, S. Liu, and R. Trivedi, Interface Sci. **10**, 217 (2002).
[17] R. E. Napolitano and S. Liu, Phys. Rev. B **70**, 214103 (2004).
[18] M. E. Glicksman and N. B. Singh, J. Phys.: Condens. Matter **98**, 277 (1989).
[19] M. Muschol, D. Liu, and H. Z. Cummins, Phys. Rev. A **46**, 1038 (1992).
[20] S. Henry, T. Minghetti, and M. Rappaz, Acta Mater. **46**, 6431 (1998).
[21] S. Henry, P. Jarry, and M. Rappaz, Metall. Mater. Trans. A **29A**, 2807 (1998).
[22] A. Sémoroz, Y. Durandet, and M. Rappaz, Acta Mater. **49**, 529 (2001).
[23] F. Gonzales and M. Rappaz, Metall. Mater. Trans. A (to be published).
[24] C. Herring, in *The Physics of Powder Metallurgy*, edited by W. E. Kingston (McGraw-Hill, New York, 1951).
[25] T. Haxhimali, A. Karma, F. Gonzales, and M. Rappaz, Nat. Mater. **5**, 660 (2006).
[26] W. R. Fehlner and S. H. Vosko, Can. J. Phys. **54**, 2159 (1976).
[27] M. Asta, J. J. Hoyt, and A. Karma, Phys. Rev. B **66**, 100101(R) (2002).
[28] C. Niederberger, J. Michler, and A. Jacot, in *Modeling of Casting, Welding and Advanced Solidification Processes XI*, edited byCh.-A. Gandin, M. Bellet, and J. E. Allison (TMS, Warrendale, 2006), p. 481.
[29] M. Rappaz, J.-L. Desbiolles, J.-M. Drezet, Ch.-A. Gandin, A. Jacot, and Ph. Thévoz, in *Modeling of Casting, Welding and Advanced Solidification Processes VII*, edited byM. Cross and J. Campbell (TMS, Warrendale, 1995), p. 449.